Application Note
SEP 2025
AN-850-0151

MMS Discovers Altered Thermal Stability of RNA, Originating from Ligand-induced Changes in Base Pairing

- ○ Biosimilars
- ○ mAbs
- ○ ADCs
- ○ AAVs
- ○ Ligand Binding
- ○ Protein/Peptide Analysis
- ○ VLPs
- ☑ Nucleic Acid
- ○ Fusion Proteins
- ○ Enzyme Analysis

- ⬢ Aggregation
- ⬢ Quantitiation
- ☑ Structure
- ☑ Stability
- ☑ Similarity

www.redshiftbio.com

Abstract

RNA structure and thermal stability are tightly linked through base pairing and stacking, which in turn governs functional processes such as transcription and translation. Ligand-induced conformational change resulted from these base-base interactions can significantly impact RNA stability, but conventional techniques fail to resolve detailed structural changes alongside thermal stability metrics. This limits the use of these techniques for structure-activity relationship (SAR) studies that are the backbone of drug development. Here, we demonstrate the use of Microfluidic Modulation Spectroscopy (MMS) to simultaneously measure RNA thermal stability and base-pair-specific structural transitions in aqueous solution. MMS was applied to a 29-mer RNA construct, containing a bulge and a hairpin, in the presence vs. absence of two small-molecule ligands. Comparison with AU- and GC-only duplexes enabled assignment of spectral features to specific base-pairing motifs. Thermal melts revealed distinct transitions at wavenumbers corresponding to base-pair disruption, while isothermal difference spectra highlighted ligand-induced enhancements in RNA structural stability. Ligand 1 induced larger structural and stability changes over a weaker-binding ligand, Ligand 2, highlighting the ability of MMS to rank compounds in SAR studies. These results establish MMS as a powerful tool for characterizing RNA-ligand interactions, offering analysis of structural and thermal stability effects that supports RNA-targeted drug discovery.

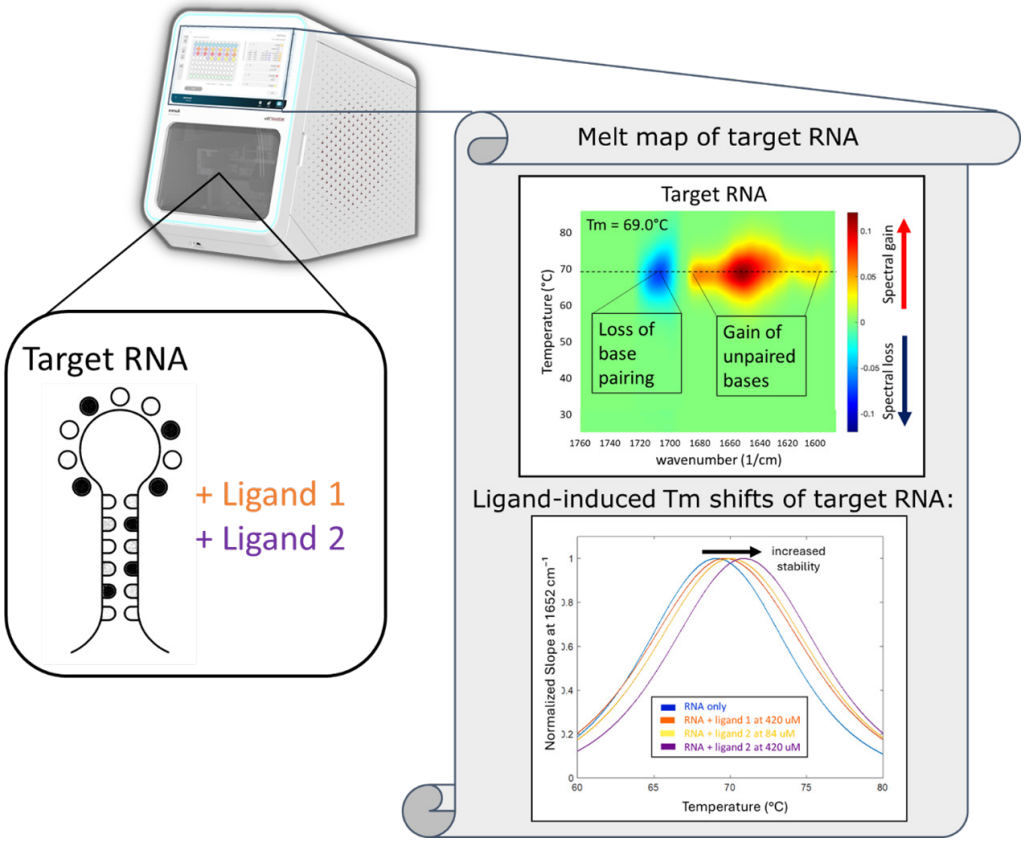

REDSHIFTBio®
80 Central Street | Boxborough MA | 01719 | info@redshiftbio.com

Application Note
SEP 2025

Introduction

RNA base pairing plays a key role in structure, guiding the formation and thermodynamic stability of helices, bulges, and loops. In turn, this structural stability determines the speed and efficiency of transcription, splicing, and translation, since structural recognition and unfolding are necessary for these processes. Small molecules that stabilize or disrupt these structural elements can shift conformational equilibria and modulate RNA function. As a result, melting temperature (T_m) has emerged as a valuable readout for evaluating ligand engagement and for guiding drug structure-activity relationship (SAR) studies targeting RNA.

Inconveniently, T_m is most easily measured using techniques that offer little or no structural insight into the biomolecule itself. Differential scanning fluorimetry (DSF) and differential scanning calorimetry (DSC) provide one-dimensional melting profiles that report on the folded and unfolded biomolecule population at each temperature, but do not distinguish specific structural elements or base-pairing motifs. Circular dichroism (CD) offers some conformational detail but suffers from narrow concentration ranges and poor buffer compatibility. Additionally, many small-molecule ligands have CD signatures, complicating the analysis or limiting the use of those ligands. While high-resolution methods such as NMR and SHAPE can detect local structural changes, they are not well-suited to thermal analysis or routine screening. There remains a need for a solution-phase method that reports on thermal stability and RNA secondary structure simultaneously.

Microfluidic Modulation Spectroscopy (MMS) is a label-free, infrared-based technique that simultaneously measures RNA structure and thermal stability in aqueous solution, offering key advantages over DSF, DSC, and CD. By tracking temperature-dependent changes in infrared spectra, MMS reveals how specific structural elements experience stabilization or destabilization due to ligand interactions, as reflected in T_m shifts at different spectral regions. This dual readout enables more detailed characterization of RNA-ligand interactions and supports structure-guided optimization in RNA-targeted drug discovery, with compatibility for automation, diverse ligand chemotypes, and a wide range of buffer excipients.

In this study, MMS was used to analyze the thermal stability and structural changes of a 29-mer RNA construct (termed "Target RNA") containing a bulge and hairpin, both in the absence and presence of two small-molecule ligands. To support spectral interpretation and confirm sequence-dependent features, model duplexes containing only AU or GC base pairs were also examined. The results demonstrate how MMS resolves base-pair-specific melting transitions and detects ligand-induced stabilization of RNA structure.

Methods

A 29-mer RNA ("Target RNA") featuring a bulge and a hairpin was diluted to 0.8 mg/mL (~80 µM) in 50 mM NaCl, 20 mM sodium phosphate, pH 6.4, and analyzed in the absence and presence of Ligand 1 (420 µM) and Ligand 2 (84 µM and 420 µM). All samples contained 0.42% DMSO final concentration as carried over from the compound concentration stock. Buffer references for each sample were prepared via sample diafiltration to match ligand and DMSO concentrations.

Two model duplexes - AU-only (5'-UUAUAUAUAUAUAA-3', PDB: 1RNA) and GC-only (5'-CCGCGG-3') - were annealed and measured at 1 mg/mL (228 µM single strand AU-only, 529 µM single strand GC-only) in 20 mM sodium phosphate, 0.5 mM EDTA, 1 M NaCl, pH 7.0. Predicted T_m values were calculated using IDT OligoAnalyzer.

All spectra were collected on the Aurora TX (RedShiftBio) from 1765 to 1588 cm^{-1} under continuous flow with thermal ramping from 25 to 95° C at 1° C/min. T_m values were extracted from the maximum of the first derivative

Results

1.) Thermal Melts of base paired constructs and Target RNA construct

Figure 1 shows MMS thermal melt maps for AU-only (1RNA, UUAUAUAUAUAUAA), GC-only (CCGCGG), and Target RNA duplexes. The AU duplex (Figure 1A) had a measured T_m of 51.8° C (predicted 59.1 °C), with major transitions at 1716, 1688, and 1652 cm^{-1}.

Application Note
SEP 2025

Results, continued

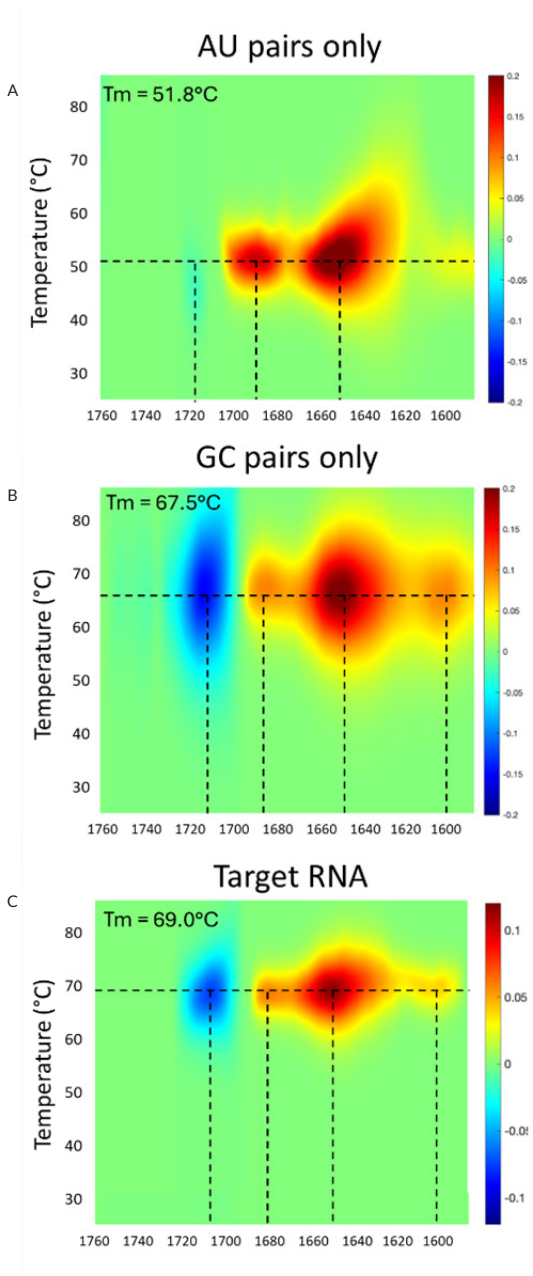

Figure 1: MMS thermal melt maps of model RNA duplexes and Target RNA. (Top) AU-only 14-mer (1RNA) with transitions at 1716, 1688, and 1652 cm^{-1} (T_m = 51.8 °C; predicted 59.1 °C). (Middle) GC-only 6-mer (CCGCGG) with transitions at 1713, 1685, 1652, and 1600 cm^{-1} (T_m = 67.5 °C; predicted 66.6 °C). (Bottom) Target RNA with transitions at 1710, 1682, 1652, and 1600 cm^{-1} (T_m = 69.0 °C). Z-axis shows first derivative spectra highlighting inflection points; transitions correspond to loss of base-paired signals (blue) and gain of unpaired peaks (red).

The GC duplex (Figure 1B) showed a T_m of 67.2 °C (predicted 66.6 °C) with transitions at 1713, 1685, 1652, and 1600 cm^{-1}. The Target RNA (Figure 1C) exhibited transitions at 1710, 1682, 1652, and 1600 cm^{-1}, yielding a higher T_m of 69.0 °C. All heat maps were generated from absolute spectra, smoothed under the assumption of a two-state transition. Concentrations were 1 mg/mL for AU and GC-only duplexes (228 and 529 µM monomer, respectively) and 0.8 mg/mL for Target RNA.

The AU duplex displayed a major thermal transition at three wavenumbers (1716 cm^{-1}, 1688 cm^{-1}, and 1652 cm^{-1}) that give a T_m of 51.8 °C, which is close to the computed T_m of 59.1 °C calculated using the IDT OligoAnalyzer (with 228 µM monomeric RNA and 1 M NaCl as the parameter set). Notably, there is some blurring of the 1652 cm^{-1} peak to lower wavenumbers during the thermal ramp, indicating that there may be an additional thermal transition for this construct. The presence of multiple thermal transitions for the AU duplex may help to explain the apparent T_m shift. Due to the tilt in the baseline and proximity of the unpaired peak for U C2=O being close to the WC base paired peak (1709 cm^{-1} vs 1712 cm^{-1}), the wavenumbers are slightly shifted in the thermal heatmap compared to their assigned positions from our previous application note (AN-850-0148).[1] In the Figure 1A, the 1716 cm^{-1} thermal transition corresponds to a loss of base paired U C2=O, the 1688 cm^{-1} transition corresponds to the growth in in-tensity at the shoulder of the unpaired U C4=O peak found at 1676 cm^{-1} , and the 1652 cm^{-1} transitions corresponds to a grown in intensity of the unpaired A NH_2 peak.

The GC duplex displayed a major thermal transition at four wavenumbers (1713 cm -1 , 1685 cm^{-1} ,1652 cm^{-1}, and 1600 cm^{-1}) that resulted in a T_m of 67.2 °C, which is very close to the T_m of 66.6 °C predicted by OligoAnalyzer (529 µM monomeric RNA and 1 M NaCl). The loss in intensity at 1713 cm^{-1} corresponds to loss of base paired G C6=O, the gain of intensity at 1685 cm^{-1} corresponds to a gain of unpaired G C6=O, the gain of intensity at 1652 cm^{-1} corresponds to a gain of unpaired C C2=O, C NH_2, and G NH_2 signal, and the gain of intensity at 1600 cm^{-1} corresponds to a gain of intensity for the unpaired G and C C=C and C=N signal.

Application Note
SEP 2025

Results, continued

The Target RNA construct (Figure 1C) displays a thermal transition at four wavenumbers (1710 cm^{-1}, 1682 cm^{-1}, 1652 cm^{-1}, and 1600 cm^{-1}) and yields a T_m of 69.0 °C. In contrast to the shorter model duplexes, the Target RNA construct has a very narrow thermal transition and has a higher T_m. These two aspects of the thermal transition are indicators of (1) more cooperative unfolding and (2) greater stability, both of which may be due to the Target RNA construct being a self-paired (folded) monomer while the AU-duplex and GC-duplex are self-complimentary dimers. Regardless, the thermal profile shown in Figure 1C is very similar to that of the GC-duplex, indicating that the paired residues in this Target RNA construct are primarily GC base pairs. Thus, for the Target RNA melt map (Figure 1C), the primary contributor to the 1710 cm^{-1} transition is the loss of paired G C6=O signal, which is converted to a gain of intensity for the unpaired G C6=O peak at 1682 cm^{-1}, the gain in intensity at 1652 cm^{-1} corresponds to the unpaired C C2=O, unpaired C NH_2, unpaired G NH_2, and likely some unpaired A NH_2, and the gain at 1600 cm^{-1} corresponds to unpaired C=C and C=N stretching modes for all four nucleobases.

2.) Isothermal Analysis of the Target RNA construct and RNA-ligand binding

Additional insights into the structural dynamics of the Target RNA construct were obtained from the inverted and baselined second derivative and the difference spectra shown in Figure 2. The top panel displays the inverted and baselined second derivative spectrum of the Target RNA construct, highlighting distinct peaks at approximately 1710 cm^{-1} (positive indicates increased G C6=O and U C2=O WC base pairing), 1682 cm^{-1} (positive indicates greater single-stranded G C6=O), 1652 cm^{-1} (Multiple groups absorb more for single stranded RNA), and 1600 cm^{-1} (C=C and C=N double bond stretching mode), which is consistent with previously observed transitions associated with base pairing. The bottom panel presents the difference spectra comparing Target RNA with samples treated with different concentrations of Ligand 1 and Ligand 2. In both cases, the 1710 cm^{-1} and 1682 cm^{-1} bands increase in intensity, suggesting that ligand binding enhances base pairing interactions within the Target RNA construct. Notably, Ligand 2 induces more pronounced spectral changes than Ligand 1, particularly with increasing concentration, indicating a concentration-dependent or saturable binding mechanism. Furthermore, at equal ligand concentrations, Ligand 2 produces a greater increase in the 1710 and 1682 cm^{-1} signals, implying that Ligand 2 more effectively stabilizes base pairing in the RNA structure compared to Ligand 1.

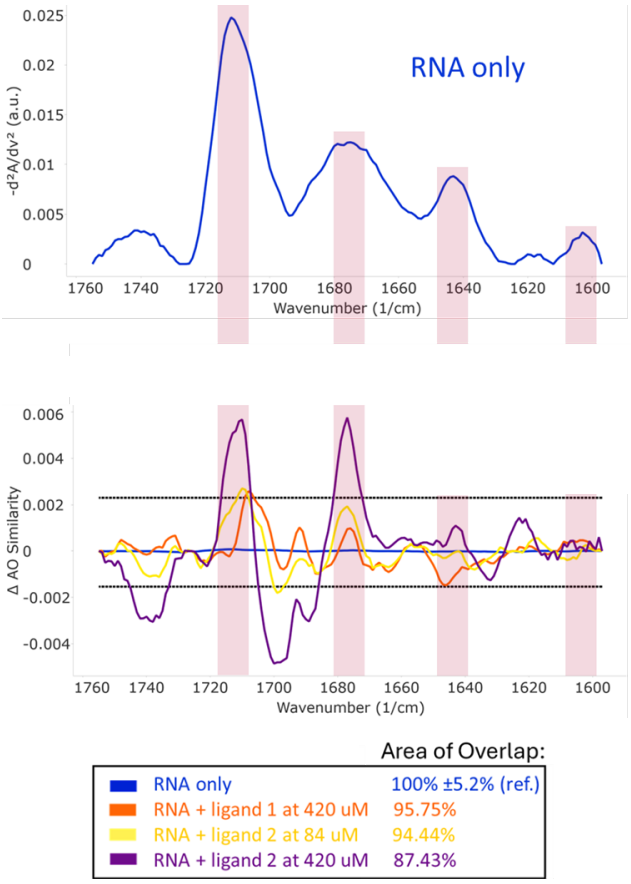

Figure 2: Second derivative and difference spectra of the Target RNA construct. Top: Inverted, baselined second derivative spectrum of the target RNA (blue), highlighting peaks at ~1710, 1682, 1652, and 1600 cm^{-1}, consistent with base pairing and single-stranded RNA signatures. Bottom: Difference spectra between pure target RNA (blue) and Ligand 1 (orange), and Ligand 2 at varying concentrations (yellow and purple). Both ligands increase 1710 and 1682 cm^{-1} signals, indicating enhanced base pairing; Ligand 2 produces larger, concentration-dependent changes, suggesting greater stabilization of RNA structure.

Application Note
SEP 2025

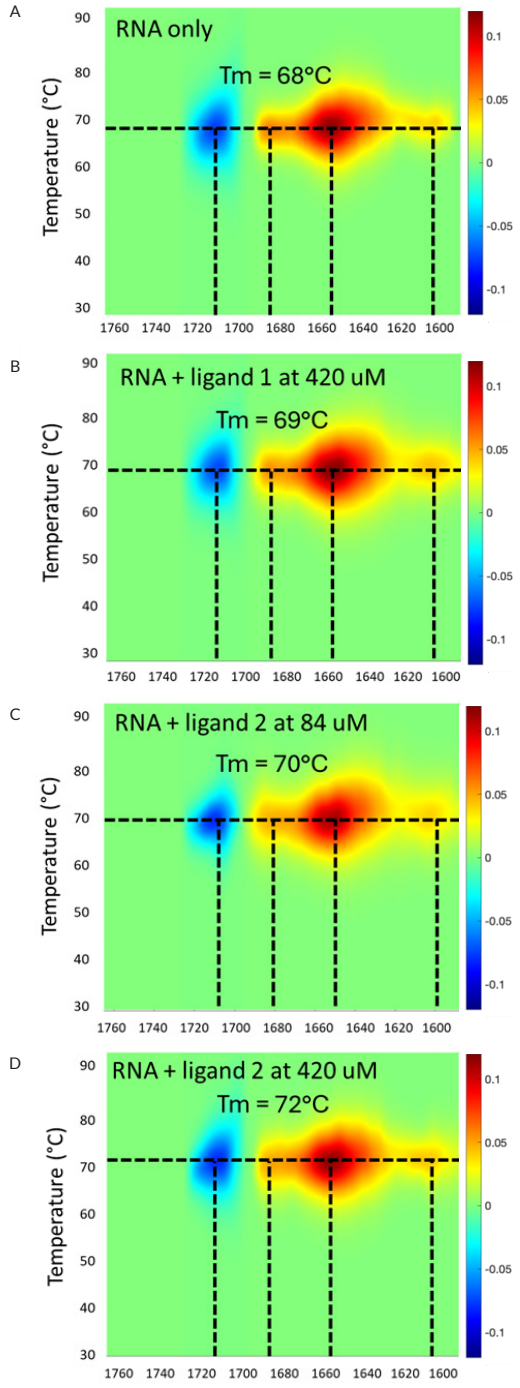

Figure 3: MMS thermal melt maps of apo and ligand-bound Target RNA. Top: Reference melt map of apo Target RNA (from Figure 1) with transitions at ~1710, 1682, 1652, and 1600 cm^{-1}. Remaining panels: Target RNA incubated with varying concentrations of Ligand 1 or Ligand 2. Melt profiles are highly similar to the apo form, indicating that ligand binding preserves overall folding and transition features. Ligand 1 and 2 increase the melting temperature T_m of the target RNA.

3.) Thermal Melts of Target RNA and different ligand interactions

Figure 3 presents MMS thermal melt maps of the apo Target RNA and Target RNA samples incubated with different concentrations of Ligand 1 and Ligand 2, corresponding to the same set of samples analyzed in Figure 2. The top panel reproduces the previously discussed Target RNA melt map from Figure 1, serving as a reference for comparison. The melt maps of the ligand-bound Target RNA samples closely resemble the apo Target RNA profile, exhibiting the same characteristic transition features at ~1710 cm^{-1}, 1682 cm^{-1}, 1652 cm^{-1}, and 1600 cm^{-1}. This strong similarity indicates that the overall folding and structural mechanism remain conserved upon ligand binding, consistent with a model in which the ligands stabilize an already existing base-paired conformation.

However, subtle shifts in the melting temperature (T_m) are observed depending on the type and concentration of ligand.

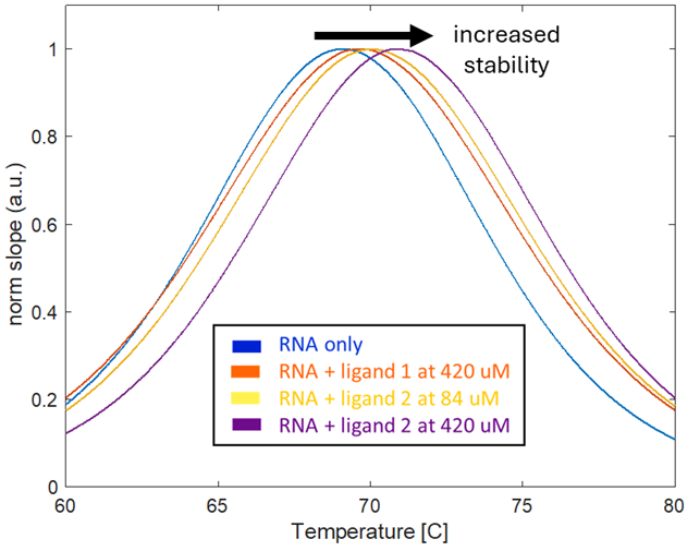

Figure 4: Melting curves of apo and ligand-bound Target RNA at 1652 cm^{-1}. Thermal profiles for apo Target RNA and samples with varying concentrations of Ligand 1 or Ligand 2 reveal subtle T_m shifts. Higher ligand concentration, especially of Ligand 2, produces slight T_m increase, consistent with enhanced base pairing and greater structural stabilization inferred from spectral analysis.

Application Note
SEP 2025

Results, continued

Figure 4 illustrates the detailed melting curves of the Target RNA and Holo RNA samples along the strongest hotspot, i.e. at 1652 cm^{-1}. These variations suggest ligand-induced modulation of RNA thermal stability, with higher ligand concentrations, particularly of Ligand 2, slightly increasing the T_m, consistent with the greater base pairing enhancement inferred from spectral analysis in Figure 2. Collectively, these data support a model in which both ligands enhance RNA base pairing, with Ligand 2 having a stronger stabilizing effect, as reflected by both spectral features and thermal behavior.

Conclusions

This study demonstrates the capability of Microfluidic Modulation Spectroscopy (MMS) to provide simultaneous and detailed insights into RNA thermal stability and structural dynamics in response to small-molecule ligand binding. By resolving wavenumber-specific melting transitions, MMS distinguishes base-pair-dependent thermal behavior in RNA constructs and reveals how ligand interactions selectively stabilize structural elements. This sets MMS apart from DSC, which has a similar sample throughput but requires roughly 2x as much material and does not provide structural information. Comparison with model AU- and GC-only duplexes allowed spectral assignment of base-pair types, while analysis of a 29-mer bulge-hairpin RNA construct showed that ligand-induced stabilization correlates with increased spectral intensity and subtle T_m shifts. Among the tested compounds, Ligand 2 exhibited greater structural stabilization effects than Ligand 1, consistent across both isothermal and thermal melt analyses. These findings validate MMS as a powerful, label-free technique for characterizing RNA-ligand interactions in solution and highlight its value for RNA analysis in general.

Contributors

Jan Schaefer, Ph.D.
Scott Gorman, Ph.D.

ZoBio (part of Oncodesign Services)
BioPartner 2, J.H. Oortweg 19,
2333 CH Leiden, Netherlands

Reference

1. Gorman, S., Huang, R. “IR Spectral Signatures of GC, AU, and GU Base Pairing in H_2O-based Buffer by Microfluidic Modulation Spectroscopy.” Application Note AN-850-0148.